SNPP VIIRS reflective solar bands on-orbit calibration six-year update: extension and improvements

J. Sun[1,2] and M. Wang[1]

[1]NOAA National Environmental Satellite, Data, and Information Service, Center for Satellite Applications and Research, E/RA3, 5830 University Research Ct., College Park, MD 20740, USA
[2]Global Science and Technology, 7855 Walker Drive, Suite 200, Greenbelt, MD 20770, USA

ABSTRACT

The Suomi National Polar-orbiting Partnership (SNPP) Visible Infrared Imaging Radiometer Suite (VIIRS) has been on-orbit for more than 6 years. VIIRS has 22 spectral bands, among which fourteen are reflective solar bands (RSB) covering a spectral range from 0.410 to 2.25 μm. The SNPP VIIRS RSB have performed very well since launch. The radiometric calibration for the RSB has also reached a mature stage after almost six years since its launch. Numerous improvements have been made in the standard RSB calibration methodology. Additionally, a hybrid calibration method, which takes the advantages of both solar diffuser calibration and lunar calibration and avoids the drawbacks of the two methods, successfully finalizes the highly accurate calibration for VIIRS RSB. The successfully calibrated RSB data record significantly impacts the ocean color products, whose stringent requirements are especially sensitive to calibration accuracy, and helps the ocean color products to reach maturity and high quality. Nevertheless, there are still many challenge issues to be investigated for further improvements of the VIIRS sensor data records (SDR). In this presentation, SNPP VIIRS RSB calibration and performance in the past six-year since launch will be presented.

Keywords: SNPP, VIIRS, RSB, SD, SDSM, Moon, SDR, Calibration, Improvements, Reprocessing

1. Introduction

The Suomi National Polar-orbiting Partnership (SNPP) Visible Infrared Imaging Radiometer Suite (VIIRS) onboard the satellite was launched on 28 October 2011 [1,2]. VIIRS has 22 spectral bands covering a spectral range from 0.410–12.013 μm. Among the 22 VIIRS channels, 14 are reflective solar bands (RSBs) with 3 imaging bands (I-bands) of higher spatial resolution and other 11 moderate resolution bands (M-bands). Among the 11 M-bands, 6 are dual-gain bands while other M-bands as well as all 3 I-bands are single-gain bands. The central wavelengths of the 14 SNPP VIIRS RSBs, their center wavelengths, key specifications, and major applications are listed in Table 1 [3]. The RSB are calibrated on-orbit with an on-board solar diffuser (SD) and a SD stability monitor (SDSM) system for RSB [4-9]. The VIIRS RSB on-orbit changes are also monitored with scheduled monthly lunar observations through the instrument's space view (SV) port [10–12], which is also used to provide the instrument's dark scene response.

Earth Observing Systems XXIII, edited by James J. Butler, Xiaoxiong (Jack) Xiong, Xingfa Gu, Proc. of SPIE Vol. 10764, 107641A · © 2018 SPIE · CCC code: 0277-786X/18/$18 · doi: 10.1117/12.2320238

Table 1. VIIRS RSB and SDSM Specification.

SDSM		VIIRS RSB			
Detector	CW (nm)	Band	CW (nm)	BW(nm)	Gain
D1	412	M1	410	20	DG
D2	450	M2	443	18	DG
D3	488	M3	486	20	DG
D4	555	M4	551	20	DG
NA	NA	I1	640	80	SG
D5	672	M5	671	20	DG
D6	746	M6	745	15	SG
D7	865	M7	862	39	DG
D7	865	I2	862	39	SG
D8	935	NA	NA	NA	NA
NA	NA	M8	1238	20	SG
NA	NA	M9	1378	15	SG
NA	NA	M10	1610	60	SG
NA	NA	I3	1610	60	SG
NA	NA	M11	2250	50	SG

CW: Center Wavelength; BW: Bandwidth; DG: Dual Gain; SG: Single Gain.

The ocean color EDR products [13-15] are highly sensitive to the accuracy of the SDR and hence to that of the RSB calibration [16]. We have demonstrated that the RSB calibration coefficients (F-factors) obtained from the SD/SDSM calibration have long-term biases, especially in short wavelength bands, due to the "non-uniformity degradation effect" of the SD and other mechanisms [17,18]. The lunar calibration does not have the long-term bias issue since the reflectance of the lunar surface is very stable in the VISible (VIS) and Near-InfraRed (NIR) spectral range [11,12]. A hybrid approach has been developed by us to combine SD-based and lunar-based calibration coefficients to generate a set of hybrid F-factors, which finally remove the long-term drifts observed in the ocean color EDR and meet the ocean color EDR's stringent requirement for the RSB calibration [21,22]. The ocean color EDR has been successfully reprocessed a couple of times with the hybrid F-factors since 2014, which significantly improves the quality and accuracy of the ocean color EDR products [20,22].

In this paper, the VIIRS RSB calibration and its improvements are briefly described, the performance of the RSB is reviewed. In Section 2, RSB SD calibration and lunar calibration improvements are reviewed and the calibration results are shown. In section 3, hybrid calibration coefficients are reviewed. Section 5 summaries and concludes the work.

2. SD and SDSM Calibration

The SNPP VIIRS SDSM calibration was performed for every orbit in the first few months on orbit, and then the operational rate was reduced to once per day, and further reduced to once every two days after 16 May 2014. So far, more than 2120 SDSM measurements have been performed for VIIRS. The SDSM has eight detectors with different center wavelengths tracking the SD degradation at the eight wavelengths which are listed in Table 1. Figure 1 shows the SD degradation derived from the SDSM measurements in symbols. They change smoothly over time except for those measured by the SDSM detectors D7 and D8, which show more noise [9]. Solid lines in Figure 1 are either the exponential functions of time fitted to the measured data (detectors D7 and D8), or the linear connections of the measured data (all other detectors). Both the symbols and solid lines are normalized at the time of launch, 28 October 2011. The solid lines for the SD degradation at eight different wavelengths and their linear

interpolations for other wavelengths within the spectral coverage are used to derive the SD F-factors [6,9]. As expected, the SD degrades faster at shorter wavelengths. In the past six plus years since VIIRS first flight, the SD has degraded about 39.0%, 31.5%, 25.7%, 17.0%, 7.7%, 5.0%, 2.5%, and 2.1% at wavelengths of 412, 450, 488, 555, 672, 746, 865, and 935 nm, respectively. The SD degradation for the shortwave infrared (SWIR) bands, or wavelengths longer than 935 nm, is beyond the spectral coverage of the SDSM, as seen in Table 1, and typically is assumed to be null for wavelengths beyond this range.

The SD is fully illuminated whenever the instrument passes the southern pole from the nightside of the Earth to dayside, as mentioned previously, generating about 14 SD calibration events daily, from which 14 sets of RSB calibration coefficients can be derived. The F-factors are calculated for each RSB, detector, gain status, and HAM side. Figures 2 shows the F-factors for bands M1 with high gain and HAM side 1, where D1, D2, . . . , and, D16 denote detector 1, 2, . . . , and 16, respectively. The F-factors are clearly detector- and time-dependent. In the last five plus years, they have changed about 3-6% for band M1. The F-factors displayed in Figure 2 are stable and the level of noises or fluctuations in them are within ~0.2%.

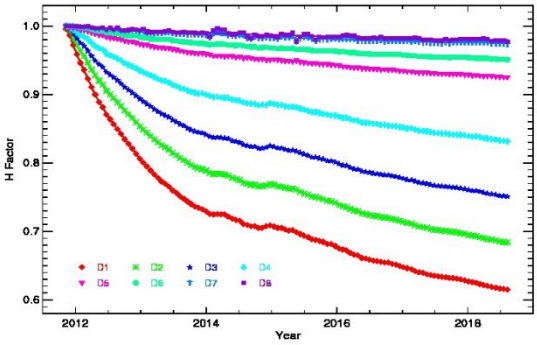

Figure 1. SNPP VIIRS SD degradation.

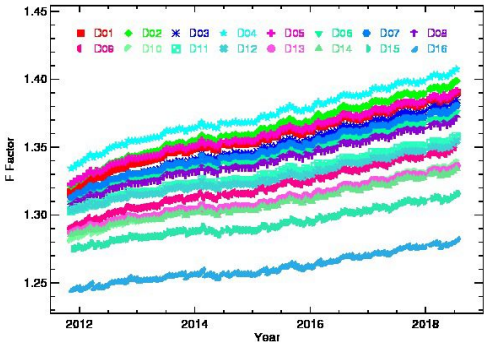

Figure 2. SNPP VIIRS band M1 high gain HAM side detector averaged SD F-factors.

The detector-averaged F-factors for VIS/NIR bands with high-gain status and HAM 1 are displayed in Figure 3. The F-factors for non-SWIR bands are normalized at the first measurement. The F-factors shown in this figure and all figures in following as well as the H-factors in Fig. 1 are the calculated values from each individually selected SD measurement without any averaging over different events. From Figure 3, it is seen that the F-factors of bands I2 and M7 have the largest increase, of about 72.0%. M6 has the second largest F-Factor increase of about 35.0%. The F-factor of band M3 has the least increase and is actually a modest decrease of about 0.5% in the last six plus years. The F-factor of band M1, which has the shortest wavelength among all RSB, has only increased ~4.5% since launch. Since VIIRS on-orbit, the F-factors of bands M2, M4, I1, and M5 have increased about 2.5%, 1.0%, 10.0%, and 16.0%, respectively. The gain of a band is inversely proportional to the F-factor of the band. Thus, the increase of a band's F-factor means the degradation of the band and a larger increase of the F-factor indicates a larger degradation of the band's gain. Generally, the NIR bands have degraded much faster than VIS bands. The degradation of the NIR bands is mainly due to the degradation of the RTA, which has the largest degradation, around a wavelength of 1000 nm [25-27]. Among bands M1-M3, which have the shortest wavelengths, the band with the shorter wavelength has the larger degradation. The degradations of these bands are mainly due to the degradation of the HAM, which degrades faster at a shorter wavelength [6].

3. Lunar Calibration

The Moon is known to have a very stable reflectance in the VIS and NIR spectral regions [29,30] and has been widely used to track the RSB on-orbit gain changes [31–33]. Since the lunar surface is not smooth, the lunar irradiance instead of the lunar radiance is used for RSB calibration [30]. The lunar irradiance strongly depends on the viewing geometry. The Robotic Lunar Observatory (ROLO) model [25,26] can provide the predicted lunar irradiance, which can be used to account for the geometric effect. The relative uncertainty of the irradiance predicted by the ROLO model over the entire view geometry is about 1% [34], which may induce a seasonal oscillation in the derived lunar F-factors. The oscillation with amplitude of ~1% or less are indeed seen in the derived SNPP VIIRS RSB lunar F-factors [11,12]. With careful analysis, we found the oscillation can be related to the lunar librations and introduced a correction based on the lunar libration angles to remove the seasonal oscillation in the lunar F-factors [21,22]. With the correction, the oscillation pattern in our lunar F-factors is removed and the uncertainty of geometric effect correction is further reduced.

The F-factors, derived for SNPP VIIRS VIS and NIR bands from the scheduled lunar observations, are shown in Figure 4 as symbols. Similar to SD F-factors, the lunar F-factors are strongly wavelength-dependent and increase with time. As expected, the largest increase occurs in the F-factors for bands I2 and M7, and changes in those for short wavelength bands are small. Among the three shortest wavelength bands M1-M3, band M1 has had the largest increase in lunar F-factors in the last four years. Compared to those reported in literature [11,12], the lunar F-factors in Figure 4 are indeed much smoother and less noisy due to the correction beyond the ROLO model prediction. The SD F-factors are also drawn in Figure 4 for VIS and NIR bands with solid lines for comparison. The lunar F-factors are normalized to the SD F-factors corresponding to the April 2012 lunar observation. It can be seen that the F-factors from the two calibrations are in general agreement but with observable differences. The differences between the two sets of F-factors also increase with time. For a more clear demonstration of the differences, Figure 5 shows only the F-factors for bands M1–M4. Among the four bands, the largest difference occurs in the band M4, which is about 2.0%, and band M3 has the second largest difference, which is about 1.7%. The differences for bands M1 and M2 are about 1.5% and 1.2%, respectively. The exact root causes of the differences between the SD/SDSM calibration and the lunar calibration are difficult to identify. However, in our previous works using both SDSM and RSB measurements from SD observations, it has been demonstrated that the SD degrades non-uniformly with respect to incident direction, especially for short wavelength bands [6,17,18]. This indicates that the SD degradation derived from the SDSM calibration may not be exactly the same as the SD degradation for the RTA view direction, resulting in errors featured as a long-term drift in the SD F-factors. The lunar calibration based on irradiance, however, faces no degradation issue and, in principle, should provide more reliable and accurate long-term RSB gain on-orbit changes. Thus, the non-uniformity of the SD degradation should be one of the main reasons for the discrepancy of the two sets of F-factors and should be the primary one for short wavelength bands.

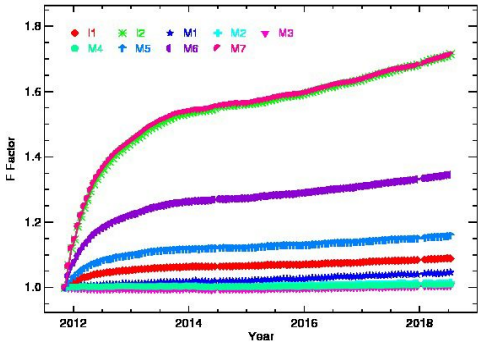

Figure 3. SNPP VIIRS RSB high gain HAM side detector averaged SD F-factors.

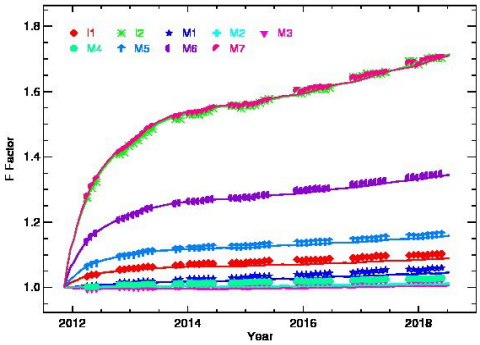

Figure 4. SNPP VIIRS detector-averaged RSB F-factors: Symbols, lunar F-factors; Solid lines, SD F-factors.

4. Hybrid RSB F-factor LUTs

SD/SDSM or lunar calibration alone has its advantages and disadvantages. Lunar calibration provides more accurate and reliable long-term VIIRS RSB on-orbit gain changes but is less frequent, only about nine times each year, and have greater measurement uncertainty due to difficulty in accurately correcting the viewing geometry effect on the lunar irradiance. On the other hand, the SD/SDSM calibration can provide VIIRS RSB on-orbit change for each orbit and is smooth and stable in a short time frame, although the derived F-factors demonstrate long-term bias due partly to the degradation non-uniformity effect [6,18]. A hybrid approach has been proposed and applied to combine the two sets of F-factors by using the lunar F-factors as the long-term baseline and the SD F-factors for short-term gain variation [21].

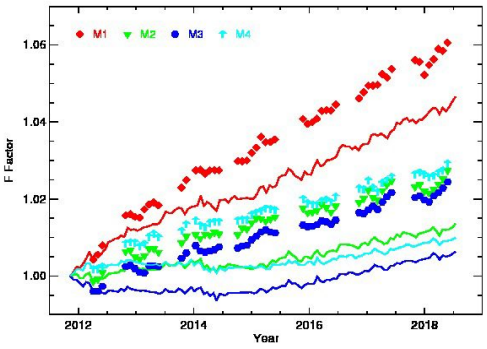

Figure 5. SNPP VIIRS detector-averaged bands M1-M4 F-factors: Symbols, lunar F-factors; Solid lines, SD F-factors.

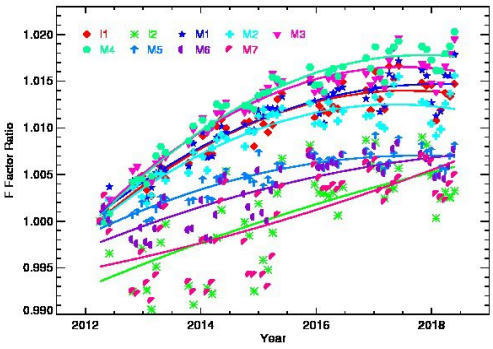

Figure 6. SNPP VIIRS F-factor ratios, lunar F-factors over SD F-factors.

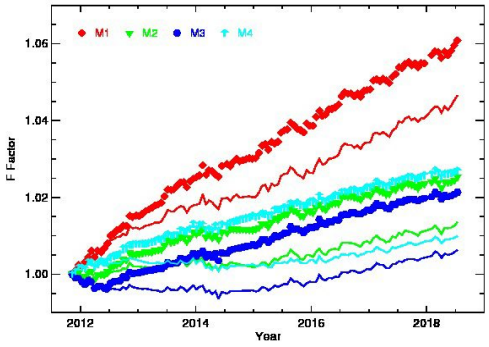

Figure 7. SNPP VIIRS detector-averaged bands M1-M4 F-factors: Symbols, hybrid F-factors; Solid, SD F-factors.

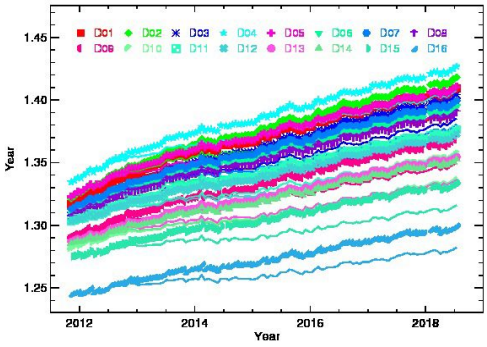

Figure 8. SNPP VIIRS detector-averaged bands M1 F-factors: Symbols, hybrid F-factors; Solid, SD F-factors.

In the hybrid approach, the ratios of the lunar factors and the SD F-factors for an RSB are calculated first, and then the ratios are fitted to a quadratic form of time. Figure 6 shows the band-averaged ratios of the two sets of F-factors and fitted functions for VIS and NIR bands, where symbols are the measured ratios and solid lines are fitted functions. It is clearly shown that the ratios are band-dependent and increase with time. The non-negligible differences between the SD and lunar F-factors for short wavelength bands are as expected according to the non-uniformity degradation of the SD. It is also noticeable that there are non-negligible differences between the two sets of F-factors for other bands with longer wavelengths. This indicates additional and unknown mechanisms contributing to the differences of the F-factors besides the non-uniformity of the SD degradation.

The hybrid F-factors are calculated by multiplying the SD F-factors and the quadratic form. The new set of F-factors averts the errors of the SD F-factors caused by the SD degradation non-uniformity effect and other unknown reasons, but keeps the frequency and smoothness of the SD F-factors. Figure 7 displays the band-averaged hybrid F-factors for bands M1-M4 and the SD F-factors. As expected, the hybrid F-factors are larger than the SD F-factors and the differences between the two sets of F-factors increase with time. It is also seen that the differences between the two sets of F-factors for the band M4 are larger than those for the other three bands. This is consistent with the ratios of the lunar and SD F-factors displayed in Fig. 7. The hybrid approach is not applied to the time period before April 2012 due to the inaccuracy of the lunar F-factors induced by the partial observations of the lunar surface [11,12].

5. Summary

The SNPP VIIRS RSB on-orbit calibration and performance in the past six years since launch are presented and reviewed. The SD degrades continuously degrades with time and degrades larger at shorter wavelength. The SD has degraded 40% at shortest wavelength of 411 nm. All RSB smoothly degrade with time as expected with largest degradation of 70% occurred at bands I2 and M7. The SD and lunar F-factors agree with each other in general but continuously diverge to each other with time for all RSB. The differences between the two sets of F-factors are band dependent. Band M4 has largest difference among all RSB, which is about 2%. The hybrid F-factors derived from the SD and lunar F-factors using a hybrid approach are presented and reviewed.

Acknowledgements

The views, opinions, and findings contained in this paper are those of the authors and should not be construed as an official NOAA or U.S. Government position, policy, or decision.

References

1. Cao, C.; Deluccia, F.; Xiong, X.; Wolfe, R.; Weng, F. Early on-orbit performance of the Visible Infrared Imaging Radiometer Suite (VIIRS) onboard the Suomi National Polar-orbiting Partnership (S-NPP) satellite. IEEE Trans. Geosci. Remote Sens. 2014, 52, 1142–1156.
2. Xiong, X.; Butler, J.; Chiang, K.; Efremova, B.; Fulbright, J.; Lei, N.; McIntire, J.; Oudrari, H.; Sun, J.; Wang, Z.; et al. VIIRS on-orbit calibration methodology and performance. J. Geophys. Res. Atmos. 2014, 119, 5065–5078.
3. Baker, N. Joint Polar Satellite System (JPSS) VIIRS Radiometric Calibration Algorithm Theoretical Basis Document (ATBD); Goddard Space Flight Center: Greenbelt, MA, USA, 2013.
4. Lei, N.; Wang, Z.; Fulbright, J.; Lee, S.; McIntire, J.; Chiang, K.; Xiong, X. Initial on-orbit radiometric calibration of the Suomi NPP VIIRS reflective solar bands. Proc. SPIE 2012, 8510.
5. Cardema, J.C.; Rausch, K.; Lei, N.; Moyer, D.I.; DeLuccia, F. Operational calibration of VIIRS reflective solar band sensor data records. Proc. SPIE 2012, 8510, 851019.
6. Sun, J.; Wang, M. On-orbit calibration of the Visible Infrared Imaging Radiometer Suite reflective solar bands and its challenges using a solar diffuser. Appl. Opt. 2015, 54, 7210–7223.
7. Hass, E.; Moyer, D.; DeLuccia, F.; Rausch, K.; Fulbright, J. VIIRS solar diffuser bidirectional reflectance distribution function (BRDF) degradation factor operational trending and update. Proc. SPIE 2012, 8510, 851016.
8. Fulbright, J.; Lei, N.K.; Chiang, K.; Xiong, X. Characterization and performance of the Suomi-NPP VIIRS solar diffuser stability monitor. Proc. SPIE 2012, 8510, 851015.
9. Sun, J.; Wang, M. Visible infrared image radiometer suite solar diffuser calibration and its challenges using solar diffuser stability monitor. Appl. Opt. 2014, 36, 8571–8584.
10. Sun, J.; Xiong, X. Solar and lunar observation planning for Earth-observing sensor. Proc. SPIE 2011, 8176, 817610.
11. Sun, J.; Xiong, X.; Butler, J. NPP VIIRS on-orbit calibration and characterization using the Moon. Proc. SPIE 2012, 8510, 85101I.
12. Xiong, X.; Sun, J.; Fulbright, J.; Z. Wang, Z.; Butler, J. Lunar Calibration and Performance for S-NPP VIIRS Reflective Solar Bands. IEEE Trans. Geosci. Remote Sens. 2016.
13. Gordon, H.R.; Wang, M. Retrieval of water-leaving radiance and aerosol optical thickness over the oceans with SeaWiFS: A Preliminary Algorithm. Appl. Opt. 1994, 33, 443–452.
14. Wang, M. Remote sensing of the ocean contributions from ultraviolet to near-infrared using the shortwave infrared bands: Simulations. Appl. Opt. 2007, 46, 1535–1547.
15. Wang, M.; Shi, W. The NIR-SWIR combined atmospheric correction approach for MODIS ocean color data processing. Opt. Express 2007, 15, 15722–15733.
16. Wang, M.; Liu, X.; Tan, L.; Jiang, L.; Son, S.; Shi, W.; Rausch, K.; Voss, K. Impact of VIIRS SDR performance on ocean color products. J. Geophys. Res. Atmos. 2013, 118, 10347–10360.

17. Sun, J., M. Chu, and M. Wang, "Degradation nonuniformity in the solar diffuser bidiretional reflectance distribution function", Appl. Opt., 55, 6001-6016 (2016).
18. Sun, J., M. Chu, and M. Wang, "An exposition on the solar diffuser degradation non-uniformity effect for SNPP VIIRS and Terra/Aqua MODIS", Proc. SPIE 9972, 99721E (2016).
19. Eplee, R.E., Jr.; Turpie, K.R.; Meister, G.; Patt, F.S.; Franz, B.A.; Bailey, S.W. On-orbit calibration of the Suomi National Polar-Orbiting Partnership Visible Infrared Imaging Radiometer Suite for ocean color applications. Appl. Opt. 2015, 54, 1984–2006.
20. Wang, M.; Liu, X.; Jiang, L.; Son, S.; Sun, J.; Shi, W.; Tan, L.; Naik, P.; Mikelsons, K.; Wang, X.; Lance, V. Evaluation of VIIRS ocean color products. Proc. SPIE 2014, 9261, 92610E.
21. Sun, J.; Wang, M. Radiometric Calibration of the Visible Infrared Imaging Radiometer Suite Reflective Solar Bands with Robust Characterizations and Hybrid Calibration Coefficients. Appl. Opt. 2015, 54, 9331–9342.
22. Sun, J. and M. Wang, "VIIRS reflective solar bands calibration progress and its impact on ocean color products", Remote Sens., 8, 194 (2016).
23. McIntire, J.; Moyer, D.; Efremova, B.; Oudrari, H.; Xiong, X. On-Orbit Characterization of S-NPP VIIRS Transmission Functions. IEEE Trans. Geosci. Remote Sens. 2015, 53, 2354–2365.
24. Sun, J.; Wang, M. On-orbit characterization of the VIIRS solar diffuser and solar diffuser screen. Appl. Opt. 2015, 54, 236–252.
25. De Luccia, F.; Moyer, D.; Johnson, E.; Rausch, K.; Lei, N.; Chiang, K.; Xiong, X.; Fulbright, J.; Haas, E.; Iona, G. Discovery and characterization of on-orbit degradation of the Visible Infrared Imaging Radiometer Suite (VIIRS) Rotating Telescope Assembly (RTA). Proc. SPIE 2012, 8510, 85101A.
26. Barrie, J.D.; Fugua, P.D.; Meshishnek, M.J.; Ciofalo, M.R.; Chu, C.T.; Chaney, J.A.; Moision, R.M.; Graziani, L. Root cause determination of on-orbit degradation of the VIIRS rotating telescope assembly. Proc. SPIE 2012, 8510, 8510B.
27. Iona, G.; Butler, J.; Guenther, B.; Graziani, L.; Johnson, E.; Kenedy, B.; Kent, C.; Lambeck, R.; Waluschka, E.; Xiong, X. VIIRS on-orbit optical anomaly—Investigation, analysis, root cause determination and lessons learned. Proc. SPIE 2014, 8510, 85101C.
28. Lei, N.; Guenther, B.; Wang, Z.; Xiong, X. Modeling SNPP VIIRS reflective solar bands optical throughput degradation and its impacts on the relative spectral response. Proc. SPIE 2013, 8866, 88661H
29. Kieffer, H.H. Photometric Stability of the Lunar Surface. Icarus 1997, 130, 323–327.
30. Kieffer, H.H.; Stone, T.C. The Spectral Irradiance of the Moon. Astronom. J. 2005, 129, 2887–2901.
31. Sun, J.; Xiong, X.; Barnes, W.L.; Guenther, B. MODIS Reflective Solar Bands On-Orbit Lunar Calibration. IEEE Trans. Geosci. Remote Sens. 2007, 43, 2383–2393.
32. Eplee, Moon Barnes, R.A.; Eplee, R.E., Jr.; Patt, F.S.; McClain, C.R. Changes in the radiometric stability of SeaWiFS determined from lunar and solar measurements. Appl. Opt. 1999, 38, 4649–4664.
33. Barnes, W., X. Xiong, R. E. Eplee, Jr., J. Sun, and C. Lyu, "Use of the Moon for Calibration and Characterization of MODIS, SeaWiFS, and VIRS", Earth Science Satellite Remote Sensing, vol. 2, New York, Springer-Verlag, pp. 98-119, 2006.